# 2nd Advanced Optical Metrology Compendium

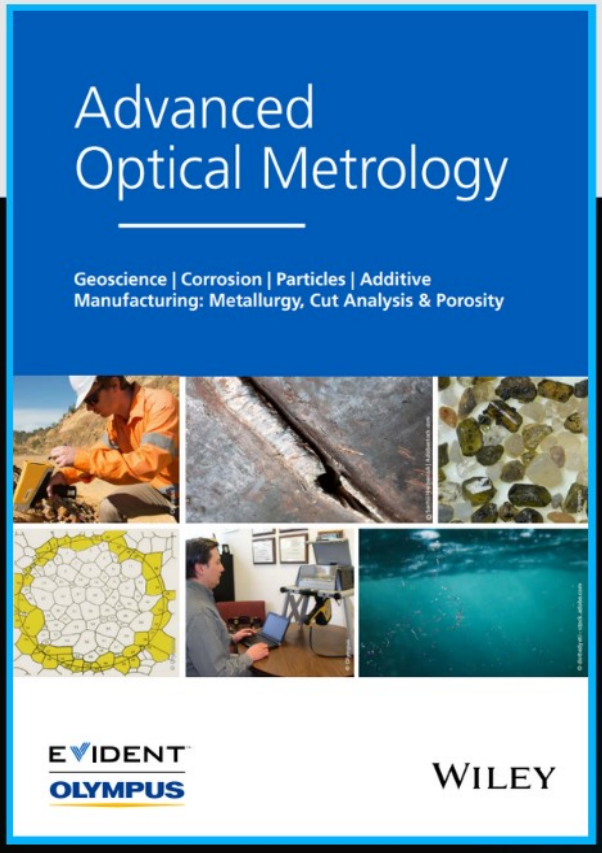


**The latest eBook from Advanced Optical Metrology. Download for free.**

This compendium includes a collection of optical metrology papers, a repository of teaching materials, and instructions on how to publish scientific achievements.

With the aim of improving communication between fundamental research and industrial applications in the field of optical metrology we have collected and organized existing information and made it more accessible and useful for researchers and practitioners.

EVIDENT™
OLYMPUS

WILEY

ADVANCED SCIENCE NEWS
www.advancedsciencenews.com



# A Phase-Separation Route to Synthesize Porous CNTs with Excellent Stability for $Na^+$ Storage

*Zhi Chen, Taihong Wang, Ming Zhang,* and Guozhong Cao**

***P**orous carbon nanotubes (CNTs) are obtained by removing $MoO_2$ nanoparticles from $MoO_2$@C core@shell nanofibers which are synthesized by phase-segregation via a single-needle electrospinning method. The specific surface area of porous CNTs is 502.9 $m^2$ $g^{-1}$, and many oxygen-containing functional groups (C—OH, C=O) are present. As anodes for sodium-ion batteries, the porous CNT electrode displays excellent rate performance and cycling stability (110 mA h $g^{-1}$ after 1200 cycles at 5 A $g^{-1}$). Those high properties can be attributed to the porous structure and surface modification to steadily store $Na^+$ with high capacity. The work provides a facile and broadly applicable way to fabricate the porous CNTs and their composites for batteries, catalysts, and fuel cells.*

Carbon nanomaterials (CNTs) have been applied in various fields, including in medicine,[1] as disinfectant,[2] in transportation,[3] and especially in energy storage in which great great attention has been attracted,[4–8] due to their low cost, chemical stability, abundance, sustainability electrical conductivity, and nontoxicity.[9–11] Although the application of carbon materials in the lithium-ion batteries (LIBs) has been commercialized, it seems that the improvement of sodium-ion batteries (SIBs) is slow due to the lack of suitable carbon nanomaterials for SIBs,[12,13] A possible reason may be that $Na^+$ is about 55% larger than $Li^+$, resulting in many materials not being about to provide enough interstitial space to hold $Na^+$, which greatly limits the application of potential candidate materials.[14–17] Therefore, the disordered carbon nanomaterials that facilitate $Na^+$ insertion/extraction appear to be suitable anode materials for the application in SIBs,[18–20] such as hard carbon with the disordered structure, which showed a capacity of 271 mA h $g^{-1}$ at 12 mA $g^{-1}$ for $Na^+$ storage,[21] but the current density is not currently satisfactory.

The mechanism of the $Na^+$ storage in a disordered structure was considered similar to that of Li,[22] and it can provide the theoretical basis for the successful application of disordered carbon in $Na^+$ storage. As Mullen and co-workers reported, porous structures of carbon nanomaterials not only effectively improve the electrochemical performance in LIBs, but also promote chemical diffusion of $Na^+$.[23] They have synthesized sandwich-like hierarchically porous carbon/graphene composites, displaying a high specific capacity of 400 mA h $g^{-1}$ at 50 mA $g^{-1}$.[24] Therefore it is necessary to obtain porous disordered carbon nanomaterials for $Na^+$ storage. At the same time, Maier has emphasized that morphology and particle size can optimize electrochemical performance, which has a crucial effect on transport $Na^+$ storage and mass transfer.[25] More recently, Ji and co-workers also showed 3D porous carbon frameworks that exhibited 99.8 mA h $g^{-1}$ after 10 000 cycles at 5 A $g^{-1}$.[10] Based on the above analysis, porous disordered carbon fibers with high specific surface areas and porosity can be a good candidate for $Na^+$ storage, especially porous CNTs which can efficiently accelerate diffusion

Dr. Z. Chen, Prof. T.-H. Wang, Prof. M. Zhang
Key Laboratory for Micro-Nano Optoelectronic Devices of Ministry of Education
School of Physics and Electronics
Hunan University
Changsha 410082, China
E-mail: zhangming@hnu.edu.cn
Prof. G.-Z. Cao
Department of Materials Science & Engineering
University of Washington
Seattle, WA 98195, USA
E-mail: gzcao@uw.edu

DOI: 10.1002/smll.201604045

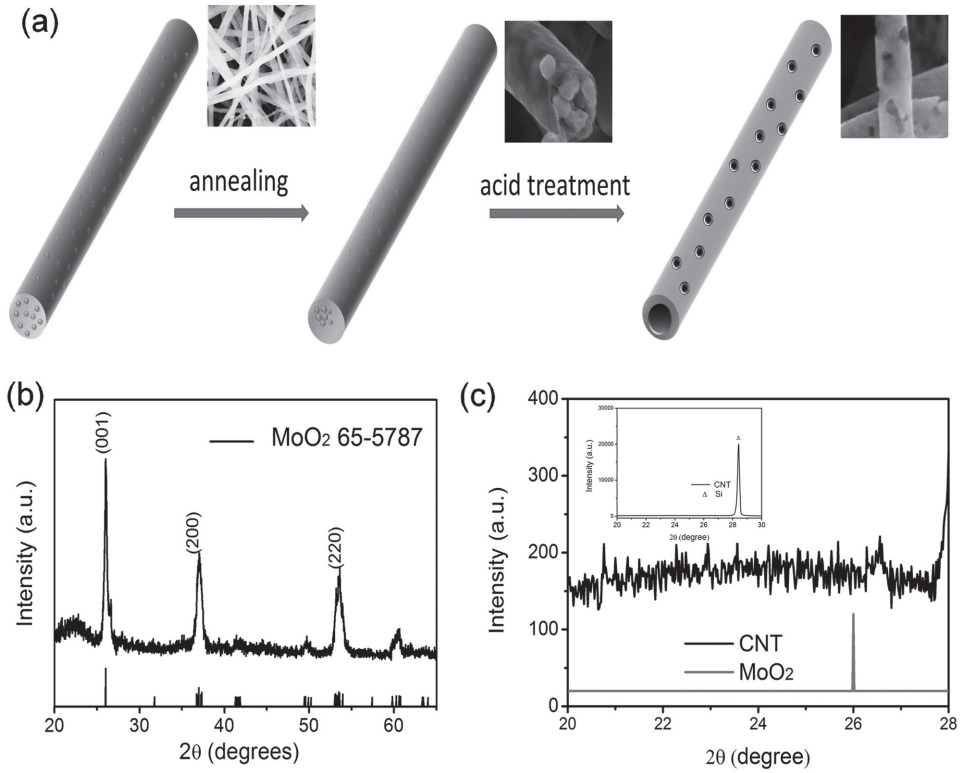


**Figure 1.** a) Schematic illustration for preparing porous CNTs, b) XRD of the product annealing at 850 °C, c) XRD of porous CNTs (Si acts as a standard).

rates for the electrolyte, and specific interface area of the electrode.[26–28]

Generally, one way to synthesize CNTs is the template method.[29,30] Suh and Lee have prepared ordered 2D carbon nanotube arrays using anodic aluminum oxide as a template.[31] The soft template method was also used to synthesize long and short carbon fibers, omitting the hard template removal process.[32,33] Another way is to synthesize CNTs by using special equipment and technology[34] (such as ALD (atomic layer deposition)). Sun and co-workers have synthesized carbon nanotubes doped with a high concentration, showing 494 mA h $g^{-1}$ at the current density of 0.1 A $g^{-1}$ for $Li^+$ storage.[35] Although these methods can efficiently fabricate CNTs, they often result in tedious or expensive synthesis procedures.

We have developed a route to synthesize porous CNTs by removing $MoO_2$ nanoparticles from $MoO_2$@C core@shell nanofibers which were obtained via single-needle electrospinning according to phase separation theory. At the same time, oxygen-containing functional groups modified on the surface of the porous CNTs can improve the wettability of the carbon nanomaterials toward the electrolyte, and form stable chemically bonded SEI (solid electrolyte interface) films, thus further enhancing the cyclic stability.[36] Therefore, the porous CNTs with disordered structure and high specific surface areas show excellent stability and high specific capacity for $Na^+$ storage.

A brief schematic to prepare porous CNTs is shown in **Figure 1**a. First, single-needle electrospinning was applied to synthesize the nanofibers with ammonium molybdate tetrahydrate (AMM) (15%) and polyvinyl alcohol (PVA). After annealing at 850 °C in Ar, the core@shell nanofibers were formed. X-ray diffractometer (XRD) was also employed to investigate the crystalline nanostructure of the core@shell nanofibers (Figure 1b). All peaks were indexed to $MoO_2$ (JCPDS: 65-5787). Then, with hot nitric acid removing $MoO_2$, the porous CNTs were obtained. XRD in Figure 1c shows that there is no characteristic peak of $MoO_2$. On the other hand, the phase-segregation may be the main driving force of thermodynamics to form $MoO_2$@C core@shell nanofibers.[37] The phenomenon was discussed in Figure S1 (Supporting Information).

In order to study the morphology of the porous CNTs, scanning electron microscopy (SEM) and transmission electron microscope (TEM) was carried out. In **Figure 2**a, it was found that $MoO_2$ nanoparticles were coated by carbon shell, forming a core @shell nanostructure. After heating treatment for 24 h, the porous CNTs were obtained in Figure 2b. And more SEM images of the $MoO_2$@C core@shell nanofibers and porous CNTs with relatively low magnification are shown in Figure S5 (Supporting Information). The resulting XRD also show that the peak of $MoO_2$ disappears, as shown in Figure 1c. At the same time, the low magnification (Figure 2c) shows that the products are porous. The HRTEM (high resolution transmission electron microscopy) of porous CNTs in Figure 2d indicates an amorphous and disordered carbon nanostructure.[38,39] Raman spectra of the porous CNTs are showed in Figure 2e, the D bands (disorder groups and defects) and G bands (sp2 carbon) are displayed at 1350 and 1600 $cm^{-1}$. The broad 2D band (≈2800 $cm^{-1}$) implies

  

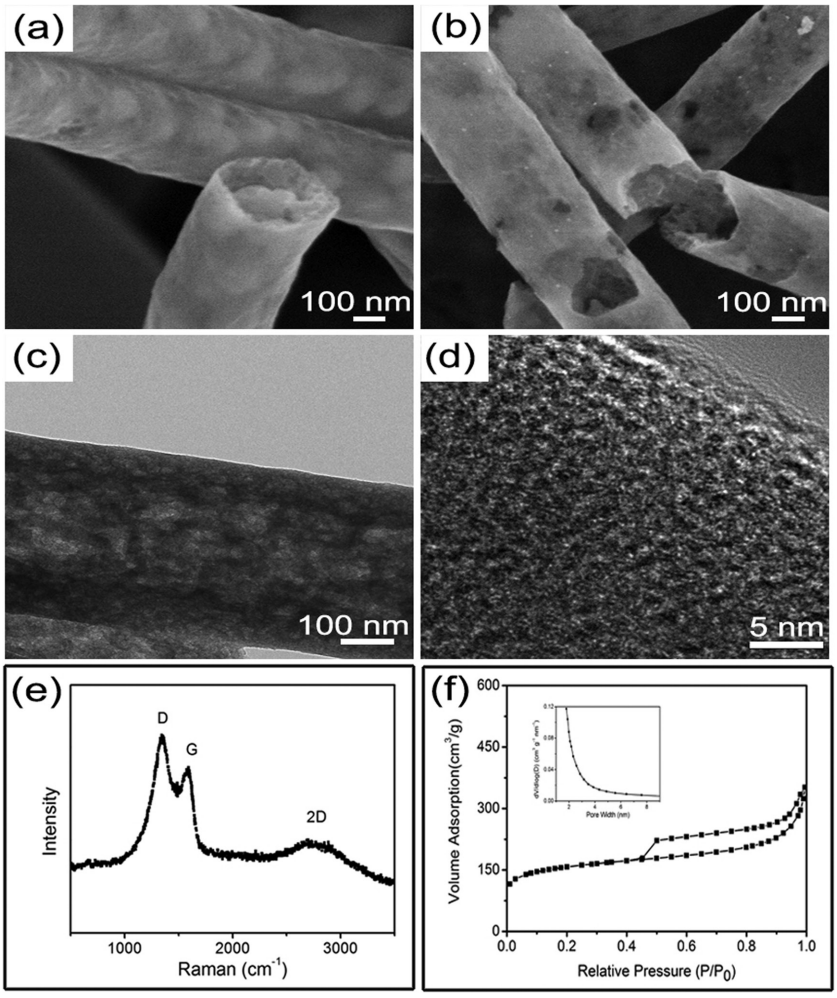


**Figure 2.** a) The image of $MoO_2$@C core@shell nanofibers annealing at 850 °C. b) The SEM image of porous CNTs with nitric acid heat treatment. c,d) The TEM, HRTEM images of porous CNTs, respectively. e) Raman spectra of the porous CNTs. f) Nitrogen adsorption/desorption isotherms of the porous CNTs (the inset is pore-size distribution).

that the porous CNTs have a good graphitization,[40] which presumably plays a major part in maintaining the integrity of the testing structure and can efficiently improve conductivity of the porous CNT electrode.[41] In addition, the N2 adsorption–desorption isotherms of the porous CNTs exhibit a type-IV isotherm associated with the presence of micropores and mesopores. The Brunauer–Emmett–Teller (BET) surface area is 502.9 $m^2$ $g^{-1}$ in Figure 2f, The porous nanostructure would provide a more favorable transportation route, while the high surface area affords more adsorption sites for $Na^+$, serving as reservoirs for $Na^+$ storage and channels for easy permeation of the electrolyte.[42]

The $MoO_2$ nanoparticles can be removed from the porous CNTs, and the surface can be also modified by the nitric acid treatment[43] to obtain oxygen-containing functional groups on the CNTs to improve the wettability of the carbonaceous material toward the electrolyte, and enabling the formation of stable chemically bonded SEI films, thus further enhancing the cyclic stability.[36,44] In order to characterize the oxygen-containing functional groups on the surface of the porous CNTs, X-ray photoelectron spectroscopy (XPS), and Fourier-transform infrared (FTIR) were analyzed in **Figure 3** and Figure S3 (Supporting Information), respectively. In Figure 3a, the porous CNTs were composed solely of carbon, oxygen, and nitrogen. Furthermore, the high-resolution C1s spectra (Figure 2b) exhibited a dominant signal corresponding to C=C at ≈284.8 eV, along with a single peak for C−N at ≈284.8 eV, and a further weaker band associated with C=O at ≈288.2 eV. The corresponding O1s spectra (Figure 2c) exhibited signals corresponding to C=O and C−OH at ≈531.5 and 533 eV, respectively. In addition, the N1s spectra showed that nitrogen, which is considered to intensify the electrical conductivity, was present in the form of oxidized N (402.6 and 406.2 eV), graphitic N (400.2 eV), as shown in Figure 2d. At the same time, the oxygen-containing functional groups were also characterized by FTIR shown in Figure S2 (Supporting Information). It was demonstrated that oxygen-containing functional groups (−OH, −C=O) existed on the surface of the porous CNTs.

CV (cyclic voltammetry) curves of porous CNT electrodes were collected at 0.25 mV $s^{-1}$ between 0 and 3.0 V to investigate the electrochemical reaction, as shown in **Figure 4**a. The clear $Na^+$ insertion peak with similar case for $Li^+$ insertion in carbon nanomaterials is located near 0 V.[45] After the second scan, the CV curves almost overlapped, indicating a good cycling stability of porous CNT electrodes during $Na^+$ insertion/extraction. The anodic peak located around 0.5 V observed in CV curves indicated $Na^+$ extraction from carbon nanomaterials. Galvanostatic charge discharge curves are described at 0.5 A $g^{-1}$ in Figure 4b. The first discapacity is 337 mA h $g^{-1}$ and the Coulombic efficiency is 67.99%. The irreversible loss may be due to formatting SEI film.[46] The rate performances of porous CNT electrodes at 0.05, 0.1, 0.2, 0.5, 1, and 2 A $g^{-1}$ are shown in Figure 4c. They deliver initial reversible discapacity of 503, 347, 291, 224, 187, and 132 mA h $g^{-1}$, still remaining at 191 mA h $g^{-1}$ after 100 cycles at 1 A $g^{-1}$. When return to 0.1 A $g^{-1}$, the porous CNT electrode still shows the capacity of 337 mA h $g^{-1}$. This result proves that the porous CNT electrode shows a good rate capability. Furthermore, cycling tests were performed to estimate the cyclability of the porous CNT electrode with different current densities. As shown in Figure 4d, the porous CNT electrode can maintain a capacity of 183.3 mA h $g^{-1}$ after 750 cycles at 0.5 A $g^{-1}$. When increased to 1 A $g^{-1}$, the initial reversible capacity possesses 224.3 mA h $g^{-1}$ and after 1000 cycles, the electrode maintains the capacity of 131.9 mA h $g^{-1}$ (Figure 4e), and the Coulombic efficiency can approach 100%

  

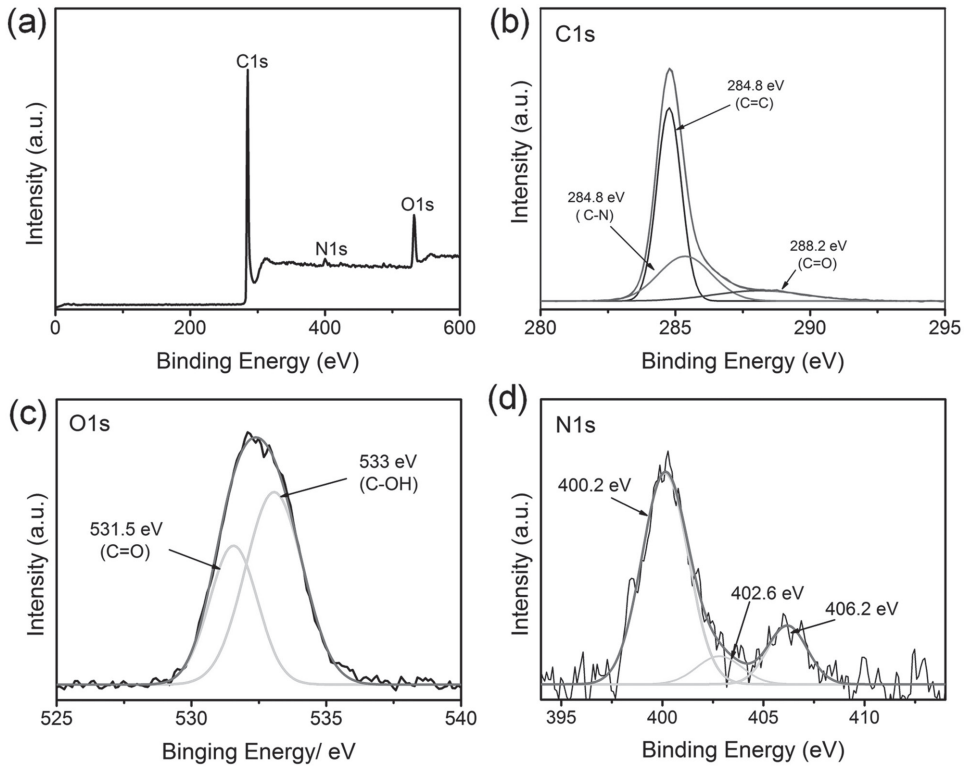


**Figure 3.** a) Low-resolution XPS spectra of porous CNFs, high-resolution XPS spectra of b) C1s, c) O1s, and d) N1s.

several cycles. In order to test the excellent performance of porous CNT electrode, after precycling at 0.5 A $g^{-1}$, the electrode can show 110 mA h $g^{-1}$ at 5 A $g^{-1}$ after 1200 cycles in Figure 4f. This result proves that the porous CNT electrode has a good stability well.

The comparison of the porous CNTs with previously reported carbon nanomaterials is shown for the application in SIBs in Table S1 (Supporting Information),[47–56] further indicating that the porous CNTs have excellent electrochemical performances for SIBs, which is attributed to the unique hollow nanostructure. First of all, the hollow carbon nanostructure guarantees efficient and continuous electron transport. Second, the porous nanostructure facilitates the migration of $Na^+$. Third, a large electrolyte/electrode contact area provides abundant active adsorption sites. Finally, oxygen-containing functional groups on CNTs improve the wettability of the carbon nanomaterial toward the electrolyte, and form stable chemically bonded SEI films, thus further enhancing the cyclic stability.[36,57]

Electrochemical impedance spectra (EIS) were used to investigate the porous CNT electrodes after different charge–discharge cycles from 100 kHz to 0.1 Hz at different cycles (Figure S3, Supporting Information). The Nyquist plot contains semicircle (high-frequency region) and the sloping straight line (low-frequency range), referring to charge-transfer resistance and diffusion impedance, respectively. It could be seen the diameters at high frequencies decrease slightly from fresh to 200 cycles, which may be due to a good infiltration of the porous CNT electrode. The corresponding charge transfer resistance ($R_{ct}$) for the porous CNT electrode decreases from 98.88 to 88.39 Ω. Although the $R_{ct}$ increases to 207.3 Ω after 500 cycles, it could be that a SEI film was generated on the surface of the electrode, so the porous CNT electrode displays a good stability, and has a capacity of 147.8 mA h $g^{-1}$ at the 500th cycle (Figure S4, Supporting Information).

$MoO_2$@C core@shell nanofibers were obtained by electrospinning with a single-needle. Then porous CNTs were obtained by subsequent nitric acid corrosion, and they have a high surface area. As anodes for SIBs, the porous CNT electrode showed excellent cycling performance and rate capacity. At 0.05 A $g^{-1}$, the electrode could display 503 mA h $g^{-1}$. When the current density was increased to 1 and 5 A $g^{-1}$, it displays capacities of 131.9 mA h $g^{-1}$ after 1000 cycles and 110 mA h $g^{-1}$ after 1200 cycles, respectively. A more simple method for the synthesis of core@shell nanostructure is introduced to research other metal oxide/carbon core@shell nanostructures.

## Experimental Section

*Porous Carbon Nanotubes*: A typical process to fabricate porous CNTs can be described as follows: AMM, ($(NH_4)_6Mo_7O_{24}\cdot 4H_2O$), PVA, and deionized water were mixed at 60 °C for 8 h to form the transparent solution, then the precursor solution was electrospun into nanofibers at the constant speed of 0.4 mL $h^{-1}$ with a DC voltage of 17 kV. The as-electrospun nanofibers were dried at 60 °C for overnight in vacuum drying box. To obtain porous CNTs, the as-electrospun nanofibers were annealed at 850 °C for 2 h in Ar. Then, the products (0.1 g) were put in the mixture of water and concentrated nitric acid (1:15, v/v). Last the as-prepared solution was transferred to a Teflon-lined stainless steel autoclave then kept at 85 °C for 20 h. The porous CNTs were washed several times, then dried at 60 °C overnight.

  

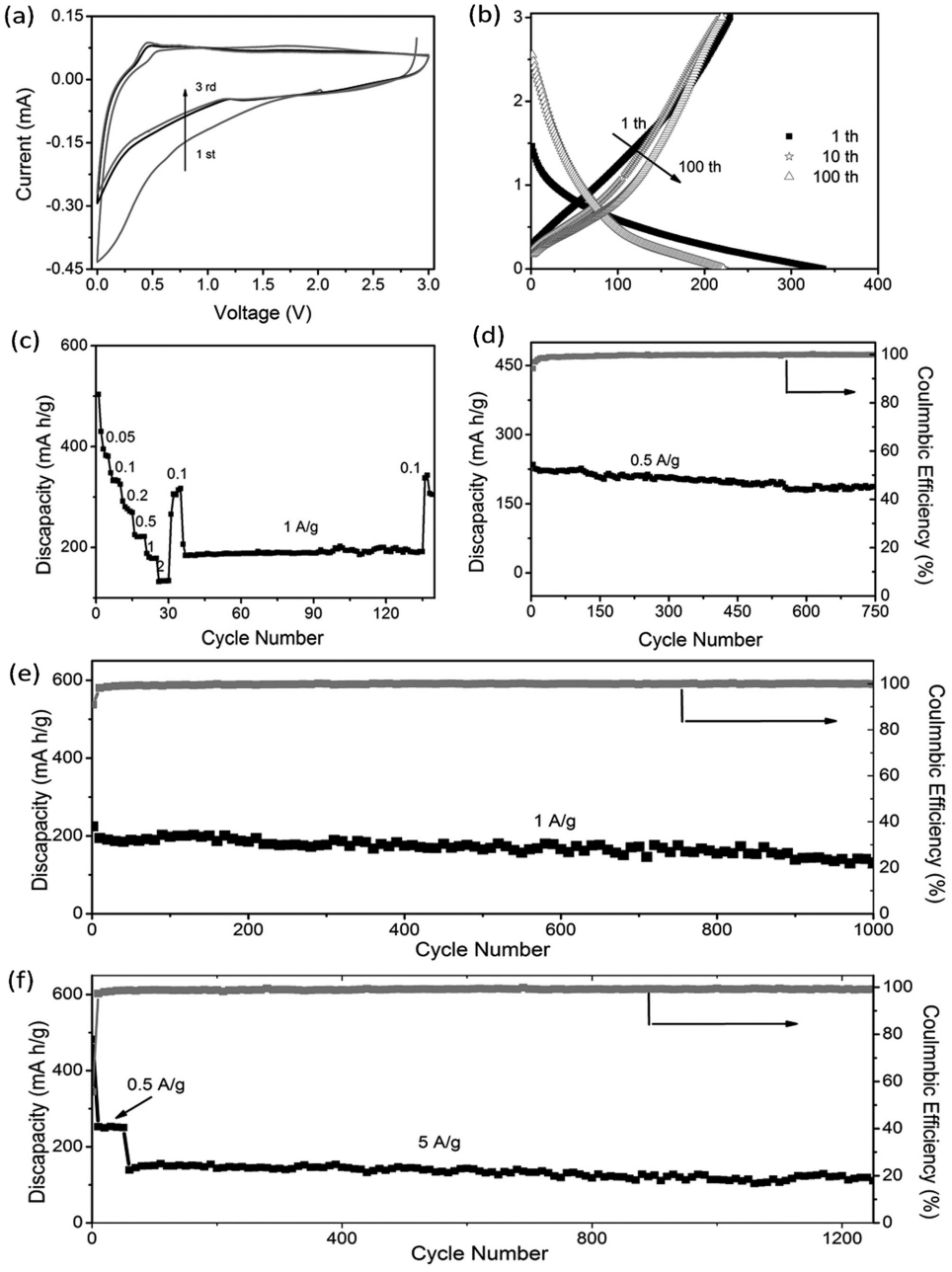


**Figure 4.** a) CV curves of the porous CNT electrode between 0 and 3.0 V at the sweep speed of 0.25 mV $s^{-1}$. b) Charge–discharge curves of porous CNT electrode at 0.5 A $g^{-1}$. c) Rate capability of porous CNT electrode at current densities of 0.05, 0.1, 0.2, 0.5, 1, and 2 A $g^{-1}$ for SIBs. d) Discharge curves of porous CNT electrode at 0.5 A $g^{-1}$, respectively. e) Discharge curves of porous CNT electrode at 1 A $g^{-1}$, respectively. f) Discharge curves of porous CNT electrode at 5 A $g^{-1}$ (after precycling at 0.5 A $g^{-1}$).

*Characterization*: The sample was characterized by XRD, a SEM (Hitachi S4-800), a TEM, the BET, Raman spectroscopy (laser wavelength of 512 nm), FTIR (AVTA-TAR, 370), XPS.

*Electrochemical Measurements*: In order to obtain a homogeneous mucus, active materials (70 wt%), conductivity agent carbon black (15 wt%), binder CMC (carboxymethyl cellulose 15 wt%) were mixed in distilled water, then stirred for 8 h. Then, the mixed gel was applied on the copper foil, then dried at 60 °C on a vacuum oven overnight. The electrolyte for SIBs was a solution of 1 M $NaClO_4$ containing PC with 3% fluoroethylene carbonate. CV curves and the EIS were obtained on a Chen Hua CHI 660E electrochemical workstation. The charge/discharge measurements were carried out on an Arbin BT2000 system with the potential window of 0–3 V.

## *Supporting Information*

*Supporting Information is available from the Wiley Online Library or from the author.*

  

## Acknowledgements

*The present work had been supported by the National Natural Science Foundation of China (Grant Nos. 51404103, 51574117, and 61376073), the Hunan University Fund for Multidisciplinary Developing (2015JCA04), and the Fundamental Research Funds for the Central Universities. This work was also in part financially supported by the National Science Foundation (NSF, DMR 1505902).*

[1] A. Bianco, K. Kostarelos, M. Prato, *Curr. Opin. Chem. Biol.* **2005**, *9*, 674.
[2] F. Hossain, O. J. Perales-Perez, S. Hwang, F. Román, *Sci. Total Environ.* **2014**, *466*, 1047.
[3] B. Liu, X. Li, B. Li, B. Xu, Y. Zhao, *Nano Lett.* **2009**, *9*, 1386.
[4] L. Dai, D. W. Chang, J.-B. Baek, W. Lu, *Small* **2012**, *8*, 1130.
[5] C. Zhang, W. Lv, Y. Tao, Q.-H. Yang, *Energy Environ. Sci.* **2015**, *8*, 1390.
[6] D. Yu, K. Goh, H. Wang, L. Wei, W. Jiang, Q. Zhang, L. Dai, Y. Chen, *Nat. Nanotechnol.* **2014**, *9*, 555.
[7] Z.-L. Wang, D. Xu, H.-G. Wang, Z. Wu, X.-B. Zhang, *ACS Nano* **2013**, *7*, 2422.
[8] H.-X. Zhong, J. Wang, Y.-W. Zhang, W.-L. Xu, W. Xing, D. Xu, Y.-F. Zhang, X.-B. Zhang, *Angew. Chem. Int. Ed.* **2014**, *53*, 14235.
[9] S. Zhu, Q. Meng, L. Wang, J. Zhang, Y. Song, H. Jin, K. Zhang, H. Sun, H. Wang, B. Yang, *Angew. Chem. Int. Ed.* **2013**, *52*, 3953.
[10] H. Hou, C. E. Banks, M. Jing, Y. Zhang, X. Ji, *Adv. Mater.* **2015**, *27*, 7861.
[11] S. Wang, S. Yuan, Y.-B. Yin, Y.-H. Zhu, X.-B. Zhang, J.-M. Yan, *Part. Part. Syst. Charact.* **2016**, *33*, 493.
[12] R. Alcantara, J. M. Jimenez-Mateos, P. Lavela, J. L. Tirado, *Electrochem. Commun.* **2001**, *3*, 639.
[13] R. Alcantara, F. J. Femandez Madrigal, P. Lavela, J. L. Tirado, J. M. Jimenez Mateos, C. Gomez de Salazar, R. Stoyanova, E. Zhecheva, *Carbon* **2000**, *38*, 1031.
[14] S. Yuan, S. Wang, L. Li, Y.-H. Zhu, X.-B. Zhang, J.-M. Yan, *ACS Appl. Mater. Interfaces* **2016**, *8*, 9178.
[15] S. Yuan, X.-L. Huang, D.-L. Ma, H.-G. Wang, F.-Z. Meng, X.-B. Zhang, *Adv. Mater.* **2014**, *26*, 2273.
[16] Y.-X. Wang, S.-L. Chou, H.-K. Liu, S.-X. Dou, *Carbon* **2013**, *57*, 202.
[17] W. Luo, C. Bommier, Z. Jian, X. Li, R. Carter, S. Vail, Y. Lu, J.-J. Lee, X. Ji, *ACS Appl. Mater. Interfaces* **2015**, *7*, 2626.
[18] D. Stevens, J. Dahn, *J. Electrochem. Soc.* **2000**, *147*, 1271.
[19] R. Alcantara, P. Lavela, G. F. Ortiz, J. L. Tirado, *Electrochem. Solid-State Lett.* **2005**, *8*, A222.
[20] X. Zhou, Y.-G. Guo, *ChemElectroChem* **2014**, *1*, 83.
[21] Y. Cao, L. Xiao, M. L. Sushko, W. Wang, B. Schwenzer, J. Xiao, Z. Nie, L. V. Saraf, Z. Yang, J. Liu, *Nano Lett.* **2012**, *12*, 3783.
[22] D. Stevens, J. Dahn, *J. Electrochem. Soc.* **2001**, *148*, A803.
[23] S. Yang, X. Feng, L. Zhi, Q. Cao, J. Maier, K. Mullen, *Adv. Mater.* **2010**, *22*, 838.
[24] Y. Yan, Y.-X. Yin, Y.-G. Guo, L.-J. Wan, *Adv. Energy Mater.* **2014**, *4*, 1301584.
[25] J. Maier, *Nat. Mater.* **2005**, *4*, 805.
[26] L. L. Zhang, X. S. Zhao, *Chem. Soc. Rev.* **2009**, *38*, 2520.
[27] S. W. Lee, J. Kim, S. Chen, P. T. Hammond, Y. Shao-Horn, *ACS Nano* **2010**, *4*, 3889.
[28] F. Valentini, A. Amine, S. Orlanducci, M. L. Terranova, G. Palleschi, *Anal. Chem.* **2003**, *75*, 5413.
[29] X. Tang, B. Zhang, C. Xiao, H. Zhou, X. Wang, D. He, *Sens. Actuators B* **2016**, *222*, 232.
[30] Z. Wen, Q. Wang, J. Li, *Adv. Funct. Mater.* **2008**, *18*, 959.
[31] J. S. Suh, J. S. Lee, *Appl. Phys. Lett.* **1999**, *75*, 2047.
[32] M. Hu, J. Reboul, S. Furukawa, L. Radhakrishnan, Y. Zhang, P. Srinivasu, H. Iwai, H. Wang, Y. Nemoto, N. Suzuki, S. Kitagawa, Y. Yamauchi, *Chem. Commun.* **2011**, *47*, 8124.
[33] Y. Zhai, Y. Dou, X. Liu, S. S. Park, C.-S. Ha, D. Zhao, *Carbon* **2011**, *49*, 545.
[34] I. Lahiri, S.-M. Oh, J. Y. Hwang, C. Kang, M. Choi, H. Jeon, R. Banerjee, Y.-K. Sun, W. Choi, *J. Mater. Chem.* **2011**, *21*, 13621.
[35] X. Li, J. Liu, Y. Zhang, Y. Li, H. Liu, X. Meng, J. Yang, D. Geng, D. Wang, R. Li, X. Sun, *J. Power Sources* **2012**, *197*, 238.
[36] Z. Shen, Y. Hu, Y. Chen, R. Chen, X. He, L. Geng, X. Zhang, K. Wu, *Small* **2016**, *12*, 5269.
[37] Z. Chen, T. Yang, H. Shi, T. Wang, M. Zhang, G. Cao, *Adv. Mater. Interfaces* **2017**, *4*, 1600816.
[38] J. Jin, Z.-Q. Shi, C.-Y. Wang, *Electrochim. Acta* **2014**, *141*, 302.
[39] P. Thomas, D. Billaud, *Electrochim. Acta* **2002**, *47*, 3303.
[40] H. Zhang, G. Zhang, Z. Li, K. Qu, L. Wang, W. Zeng, Q. Zhang, H. Duan, *J. Mater. Chem. A* **2016**, *4*, 10585.
[41] L. Jiao, L. Zhang, X. Wang, G. Diankov, H. Dai, *Nature* **2009**, *458*, 877.
[42] L. Wang, C. Yang, S. Dou, S. Wang, J. Zhang, X. Gao, J. Ma, Y. Yu, *Electrochim. Acta* **2016**, *219*, 592.
[43] K. A. Worsley, I. Kalinina, E. Bekyarova, R. C. Haddon, *J. Am. Chem. Soc.* **2009**, *131*, 18153.
[44] F. Zhou, S. Xin, H.-W. Liang, L.-T. Song, S.-H. Yu, *Angew. Chem. Int. Ed.* **2014**, *53*, 11552.
[45] T. Zheng, J. S. Xue, J. R. Dahn, *Chem. Mater.* **1996**, *8*, 389.
[46] K. Tang, R. J. White, X. Mu, M.-M. Titirici, P. A. van Aken, J. Maier, *ChemSusChem* **2012**, *5*, 400.
[47] J. Ding, H. Wang, Z. Li, A. Kohandehghan, K. Cui, Z. Xu, B. Zahiri, X. Tan, E. M. Lotfabad, B. C. Olsen, D. Mitlin, *ACS Nano* **2013**, *7*, 11004.
[48] K. Tang, L. Fu, R. J. White, L. Yu, M.-M. Titirici, M. Antonietti, J. Maier, *Adv. Energy Mater.* **2012**, *2*, 873.
[49] C. Bommier, W. Luo, W.-Y. Gao, A. Greaney, S. Ma, X. Ji, *Carbon* **2014**, *76*, 165.
[50] T. Chen, Y. Liu, L. Pan, T. Lu, Y. Yao, Z. Sun, D. H. Chua, Q. Chen, *J. Mater. Chem. A* **2014**, *2*, 4117.
[51] L. Fu, K. Tang, K. Song, P. A. van Aken, Y. Yu, J. Maier, *Nanoscale* **2014**, *6*, 1384.
[52] Y. Liu, F. Fan, J. Wang, Y. Liu, H. Chen, K. L. Jungjohann, Y. Xu, Y. Zhu, D. Bigio, T. Zhu, C. Wang, *Nano Lett.* **2014**, *14*, 3445.
[53] Z. Wang, L. Qie, L. Yuan, W. Zhang, X. Hu, Y. Huang, *Carbon* **2013**, *55*, 328.
[54] Y. Shao, J. Xiao, W. Wang, M. Engelhard, X. Chen, Z. Nie, M. Gu, L. V. Saraf, G. Exarhos, J.-G. Zhang, J. Liu, *Nano Lett.* **2013**, *13*, 3909.
[55] Q. Fan, W. Zhang, J. Duan, K. Hong, L. Xue, Y. Huang, *Electrochim. Acta* **2015**, *174*, 970.
[56] D. Li, L. Zhang, H. Chen, L.-X. Ding, S. Wang, H. Wang, *Chem. Commun.* **2015**, *51*, 16045.
[57] D. Wang, K. Wu, L. Shao, M. Shui, R. Ma, X. Lin, N. Long, Y. Ren, J. Shu, *Electrochim. Acta* **2014**, *120*, 110.

Received: December 5, 2016
Revised: January 15, 2017
Published online: March 20, 2017

  